**Bulletin of Electrical Engineering and Informatics**
Vol. 15, No. 4, August 2026, pp. 3375~3386
ISSN: 2302-9285, DOI: 10.11591/eei.v15i4.11047 

# Design and realization of X-band wideband directional coupler using elliptical multilayer substrate architecture

**Shilpa Ankit Rana[1], Ashish Kalubhai Sarvaiya[2]**
[1]Gujarat Technological University, Ahmedabad, India
[2]Department of Electronics and Communication, Government Engineering College, Gujarat, India

**Article Info**

***Article history:***

Received Jul 16, 2025
Revised Apr 10, 2026
Accepted Jul 9, 2026

***Keywords:***

Ansys
Directional coupler
Microwave system
Multilayer substrate
Power divider
Wideband
X-band

**ABSTRACT**

This paper presents the design analysis and realization of a wideband directional coupler tailored for X-band microwave applications. Directional couplers are critical components in modern microwave systems, where wide bandwidth and compact size are essential. The proposed design employs a multilayer configuration using TLY-5 substrate (epsilon r=2.20 and tangent delta=0.003), with a thickness of 0.508 mm and 17 µm copper cladding. The coupler is designed and simulated using Ansys high frequency structure simulator (HFSS) and subsequently fabricated for performance validation. It achieves a coupling factor of 3.5±0.6 dB across the 7–14 GHz range, with a transmission loss of 2.9±0.5 dB. Both return loss and isolation consistently exceed 20 dB throughout the operational band. The design exhibits a fractional bandwidth (FBW) of 66.67%, confirming its broadband capability. With a compact footprint of 2.475 lambda g ×1.485 lambda g, the coupler offers reasonable impedance matching and broadband performance, making it well-suited for integration in microwave circuits, particularly in variable attenuators and wideband communication systems.



***Corresponding Author:***

Shilpa Ankit Rana
Gujarat Technological University
Ahmedabad, India
Email: shilparana7187@gmail.com

## 1. INTRODUCTION

Directional couplers are four-port passive microwave components used for power division, signal sampling, monitoring, radar, and antenna-feed networks. Their applications also include partial-discharge sensing in gas-insulated substations [1] and compact ultra-wideband (UWB) operation using broadside-coupled microstrip lines with an elliptical ground slot [2]. Planar coupler structures, miniaturization methods, multiband techniques, and reconfigurable configurations were comprehensively reviewed in [3].

Several planar configurations have subsequently been introduced to improve bandwidth, coupling stability, isolation, compactness, and harmonic suppression. A wideband branch-line coupler using T-shaped transmission lines and open stubs was developed for 5G applications [4]. Compact broadband coupling at Ka-band frequencies was achieved through a cross-shaped groove-gap-waveguide coupling region [5]. For X-band operation, improved isolation was obtained by modifying the substrate-integrated waveguide (SIW) aperture and introducing additional metallic via rows [6]. Miniaturization was achieved using composite microstrip–coplanar-waveguide lines printed on opposite substrate surfaces and interconnected through vias [7]. A specialized planar transmission line was employed in a rat-race coupler to reduce the occupied area and suppress higher-order harmonics [8], [9]. An equivalent π-network of high-impedance lines and open-circuited stubs was employed in a WiMAX branch-line coupler in [10]. Wideband matching was obtained by loading a branch-line configuration with four open-circuited coupled lines [11]. Tight coupling, bandwidth enhancement, and size reduction were achieved using a two-section microstrip-slot branch-line coupler with overlapped open-circuited lines [12]. Harmonic suppression and substantial miniaturization were obtained by incorporating T-shaped resonators, open stubs, cross-shaped resonators, and radial stubs [13]. Nevertheless, conventional microstrip directional couplers remain affected by limited bandwidth and reduced directivity because of unequal even and odd mode phase velocities [14].

A wideband multilayer quadrature hybrid coupler using butterfly-shaped resonators was presented in [15], although multiple substrate layers, conductive layers, coupling apertures, and via fences were required. A two-layer substrate-integrated gap-waveguide coupler employing an elliptical slot and tuning vias was developed in [16]. A high-power variable dual-directional coaxial coupler with movable loop-type coupling elements was reported for 50–500 MHz operation in [17]. A double-layer SIW coupler with transverse rectangular slots was developed for phased-array feed networks, with coupling controlled through the slot dimensions and quantity [18]. A weak-coupling HMSIW coupler intended for Ku-band power detection was investigated in [19]. Multilayer SIW six-port junctions with embedded resistive films were presented in [20]; however, these structures represent complete six-port systems rather than standalone four-port couplers.

High-directivity and low-loss couplers based on empty substrate-integrated coaxial-line technology were developed in [21], although multilayer alignment, transitions, and fabrication tolerances influenced the measured response. A transformer- and ferrite-core-based coupler was reported for high-power, low-frequency monitoring applications in [22]. A folded-SIW phase shifter incorporating complementary split-ring resonators was applied to a compact 180° directional coupler in [23]. A multi-section microstrip coupler providing exceptionally broad sub-6-GHz UWB operation was presented in [24], but its coupling level remained weaker than that required for near-equal power division. Finally, an electronically tunable HMSIW coupler with adjustable coupling was demonstrated in [25], although its operating band remained below the X-band. Collectively, these studies reveal a continuing need for a tightly coupled multilayer coupler that simultaneously provides broad X-band coverage, high isolation, stable transmission characteristics, and practical fabrication.

This work presents a wideband multilayer directional coupler implemented on Rogers TLY-5 substrate for X-band applications considering the challenges discussed in the previous paragraphs. The presented coupler achieves a fractional bandwidth (FBW) of 66.67% over 7–14 GHz, with a coupling factor of 4.0±0.5 dB and insertion loss of 2.5±0.5 dB, although maintaining return loss and isolation greater than 20 dB at the center frequency. The design also exhibits a compact size of 2.475 λg×1.485 λg, making it suitable for integration into broadband microwave circuits. Full-wave high frequency structure simulator (HFSS) simulations and measurements on a designed prototype confirm the practical feasibility of the proposed structure. The remainder of this paper is organized as follows: section 2 presents the proposed coupler design and simulation methodology. Section 3 discusses the simulated and experimental results and provides a comparative performance analysis. Section 4 concludes the paper and highlights the main findings and potential future scope.

## 2. METHOD

The research methodology follows a structured sequential process, as illustrated in Figure 1. It begins with the conceptual design of a broadband directional coupler operating over 7–14 GHz with a target coupling factor of approximately -3 dB. Based on the UWB aperture-coupling approach reported in [2], a multilayer elliptical topology was selected to achieve compact size, effective coupling control, and wide bandwidth.

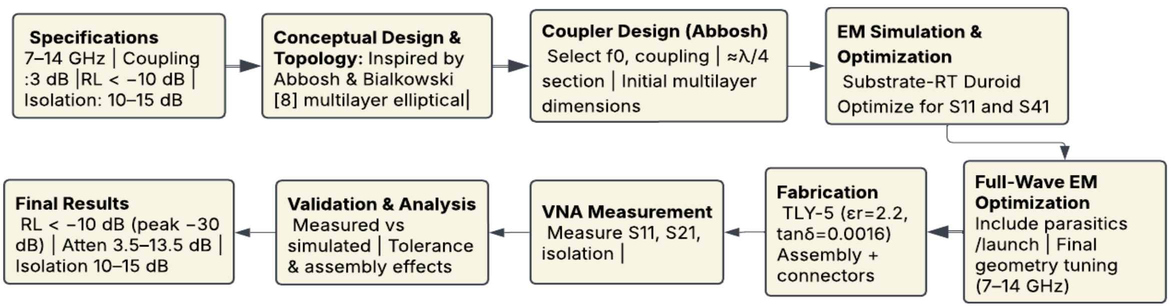


Figure 1. Methodological flow of the proposed coupler from concept to experimental validation

### 2.1. Proposed work

The geometry of the proposed coupler is illustrated in Figure 2. Figure 2(a) shows the layer arrangement and port configuration. The structure comprises three metallic layers—top, middle, and bottom—separated by two dielectric substrates. Ports 1 and 4 are located on the top conductor, whereas Ports 2 and 3 are positioned on the bottom conductor. Electromagnetic coupling between the conductors is achieved through elliptical slots etched in the top and bottom metallic layers. The design was implemented in Ansys HFSS on an RT duroid 5880 substrates with εr=2.2, thickness h=0.508 mm, copper thickness of 17 µm, and loss tangent tanδ=0.0009. The overall size of the coupler is 2.475 λg×1.485 λg, Figures 2(b) and (c) show the dimensional parameters of the outer and middle layers, respectively, with the optimized geometrical parameters are A=25 mm, B=20.5 mm, C=0.6 mm, D=2.7 mm, E=10.3 mm, G=1 mm, H=1.67 mm, I=3.8 mm, J=1.3 mm, K=5.4 mm, and M=1.4 mm. After conceptualization, the design was translated into a full-wave EM model and iteratively optimized through parametric analysis until the desired performance was achieved. The optimized design was then fabricated using a standard multilayer printed circuit board (PCB) process and assembled with connectors. Finally, the prototype was characterized using a calibrated vector network analyzer (VNA), and the measured S-parameters were analyzed, compared with simulations, and benchmarked against existing state-of-the-art designs to validate the performance and practical utility of the proposed coupler.

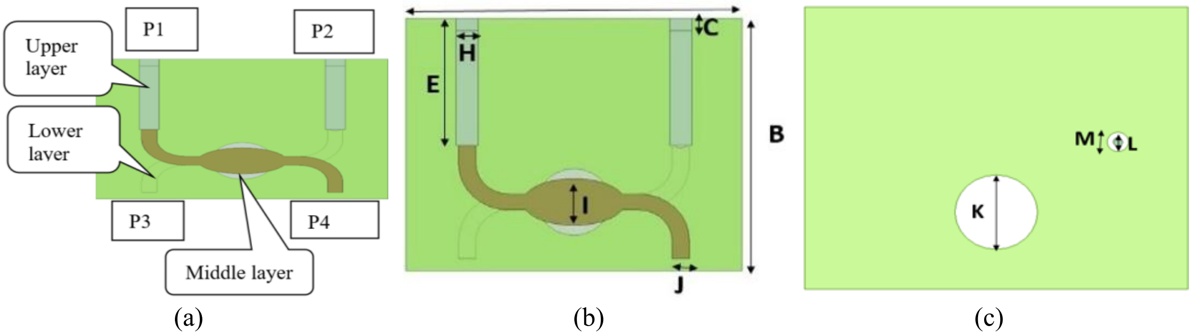


Figure 2. Proposed multilayer directional coupler; (a) layer layouts and port configuration, (b) dimensions of the top and bottom layers, and (c) dimensions of the middle layer with the circular coupling slot

### 2.2. Mathematical analysis

The sub miniature version A (SMA) ports connections are made from curved microstrip lines. By compressing the curved microstrip line to assume zero length, the structural features located in the slot have two-fold symmetry with respect to the horizontal plane and the vertical plane. If only the horizontal plane of symmetry is used to propose analysis and design of this connection. Ports 1 and 3 can have even-odd mode access, which can use circuit analysis. The two elliptical conducting patches and their rectangular equivalent approximate the slot to simplify the initial analysis and design process. The rectangular slot width denoted by $s_o$ and length denoted by $m_o$. A rectangular microstrip of width denoted by $s_q$ and length denoted by $m_n$, respectively. The coupler requires a $B_{DB}$ coupling. The odd even method is calculated as (1) and (2):

$$Y_{eo} = Y_e \left(\frac{1+10^{-B/20}}{1-10^{-B/20}}\right)^{0.5} \quad (1)$$

$$Y_{aa} = Y_e \left(\frac{1-10^{-B/20}}{1+10^{-B/20}}\right)^{0.5} \quad (2)$$

where $Y_{eo}$ represent as odd, $Y_{aa}$ represent as even characteristic impedances, and $Y_e$ represent as characteristic impedance of the microstrip port coupler. Assume that coupling $B_{DB}$ is $6\,dB$ and $Y_e = 50\,\Omega$. The slot is converted into a perfect electric conductor to while excited in the odd mode. The standard equation of the microstrip transmission line is determine width $m_n$ and realizing odd characteristic impedances. In the odd mode, the electric field through the region created in the parallel plate is mostly concentrated in the junction and ground plane. For low characteristic impedance, the fringe effect is less pronounced because compared to the substrate thickness $t$ is large to the length of the rectangular microstrip. In even mode, wave excitation occurs in a different wave propagation condition. The ground plane is replacing the slot magnetic conductor. In even mode, as the slot in the magnetic conductor uniformly shifts to the ground plane, an electric field is pushed from the parallel-plate region initiated from the microstrip port, which is due to magnetic conduction. The bottom plate cannot be formed by an electric field perpendicular to its surface due to magnetic conduction. This results in an even-mode wave exiting the plate parallel to the two antipodal slots in the microstrip port, which is formed by the ground region and elliptical patches. The dimensions of an equilateral rectangle are $s_o$ and $s_q$ shaped coupler, which provides a standard approach to the required $Y_{eo}$ even and $Y_{aa}$ odd mode characteristic impedances, as (3) dan (4):

$$Y_{eo} = \frac{60\pi}{\sqrt{\xi_p}} \frac{J(j_1)}{J'(j_1)} \quad (3)$$

$$Y_{aa} = \frac{60\pi}{\sqrt{\xi_p}} \frac{J'(j_2)}{J(j_2)} \quad (4)$$

It appears as a ratio of elliptic functions, which is roughly calculated as (5):

$$\frac{J(j)}{J'(j)} = \begin{cases} \dfrac{\frac{2}{\pi} ln\left(2\sqrt{\frac{1+j}{1-j}}\right), for 0.707 \le j \le 1}{\frac{2}{\pi} ln\left(2\sqrt{\frac{1+\sqrt{1+j}}{1_{-}\sqrt{1+j}}}\right), for 0 \le j \le 0.707} \end{cases} \quad (5)$$

where $J'(j_1) = J(\sqrt{1-j^2})$ and $J(j_1)$ represent as first kind elliptical integral, $j_1$ and $j_2$ is the parameter that is calculated as (6) and (7):

$$j_1 = \sqrt{\frac{sinh^2(\pi s_o/4t)}{sinh^2(\pi s_o/4t) + cosh^2(\pi s_q/4t)}} \quad (6)$$

$$j_2 = tanh(\pi s_q/4t) \quad (7)$$

where the substrate thickness is denoted by $t$, top and bottom microstrip patches width is denoted by $s_q$, and slot width is denoted by$s_o$. Set up the function to determine $s_q$ and $s_o$ for given values is accomplished in $Y_{eo}$ and $Y_{aa}$ using the Gauss–Newton iteration method.
The determination of the coupler length is the final stage in the coupler design procedure described in (8):

$$m_0 = m_n = {}^{\lambda_f}/_{4} \quad (8)$$

where $\lambda_f$ effective wavelength for the microstrip line. The dimensions of the ellipse are the next step in this process. Due to the small size, the dimension can be equal or the same performance can be expected for rectangular and elliptical, less than a quarter of the equivalent area in an efficient wavelength-shaped coupler. The width of microstrip in elliptical-shaped coupler $D_1$, width of the slot elliptical-shaped coupler is $D_2$, and the elliptical coupler's length is equal to that of its rectangular equivalent, which is represented by the symbol $D_3$, which is obtained as (9)-(11):

$$D_1 \approx {}^{(s_q \times m_q)}/_{C_3} \quad (9)$$

$$D_2 \approx {}^{(s_o \times m_o)}/_{C_3} \quad (10)$$

$$D_3 = \frac{\left(\sqrt{m^2{}_n + s^2{}_q + m^2{}_n}\right)}{2} \quad (11)$$

The dimensions $D_1, D_2$, and $D_3$ are finally adjusted by iteration. The finite element method runs Ansys HFSS to design and analysis package. The coupler is tested by connecting the coupler ports to SMA coaxial connectors. The coupler uses curved microstrip lines to minimize reflections.

## 3. RESULTS AND DISCUSSION

The practicality of the proposed elliptical multilayer directional coupler was assessed by full-wave electromagnetic models and experimental observations. Critical factors like return loss, isolation, insertion loss, and coupling factor were evaluated to determine the device's appropriateness for X-band applications. The findings are explained in the subsequent subsections.

### 3.1. Simulation results

The proposed elliptical multilayer directional coupler is designed and analysed using Ansys HFSS over the X-band frequency range of 7–14 GHz. The central frequency of operation is 10.5 GHz. The coupler is simulated using RT/duroid 5880 as the substrate, with a dielectric constant of εr=2.2, loss tangent (tanδ)=0.0009, substrate thickness of 0.508 mm, and copper cladding of 17 μm.

#### 3.1.1. Simulation results with variation of $D_2$

The proposed elliptical multilayer directional coupler is developed and tested using Ansys HFSS on frequencies ranging from 7 to 14 GHz, with a center frequency of 10.5 GHz. The performance is fully evaluated by looking at the S-parameters for return loss ($S_{11}$), isolation ($S_{21}$), transmission loss ($S_{31}$), and coupling factor ($S_{41}$). With $D_1$ held constant at 3.8 mm, a parametric sweep is performed for slot diameter $D_2$, which ranged from 3.8 mm to 8.8 mm, to investigate the impact of the elliptical slot geometry. The results are shown in Figures 3 and 4.

Figure 3(a) shows the input return loss at port 1 versus frequency graph for the simulated design. The y-axis shows the values of return loss, and x-axis represents the frequency from 7-14 GHz. From the figure, it can be inferred that return loss gets a lot better when the ratio $D_2/D_1$ is between 1.9 and 2.3. For the design of the coupler, the graph with $D_2$=7.3 mm has the best performance; the return loss is 20 dB at the center frequency and better than 15 dB across the 7–14 GHz band.

Figure 3(b) illustrates the isolation between Ports 1 and 2. Isolation loss refers to the unwanted coupling of power into the isolated port. The graph shows the value of isolation in dB versus the frequency spanned from 7-14 GHz. It can be observed that the isolation also shows better results for $D_2$=7.3 mm to 8.8 mm. The best isolation performance of 22 dB at center frequency is achieved when $D_2$=7.3 mm, with values consistently below 16.5 dB across the band.

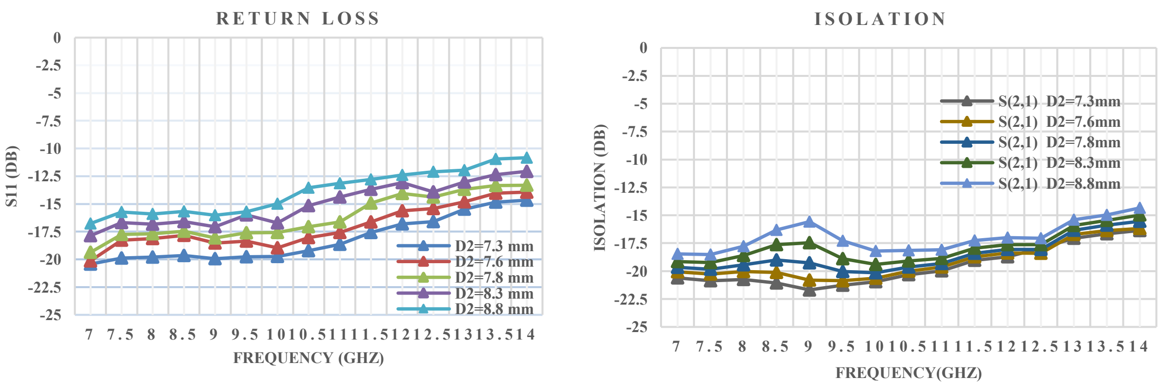


(a) (b)

Figure 3. Comparative plots of simulated; (a) return loss ($S_{11}$) and (b) isolation ($S_{21}$) for the designed directional coupler for different values of slot diameter $D_2$

In Figure 4(a), the graph is illustrated between the transmission loss at the direct port (Port 3) and frequency from 7-14 GHz. It has been observed that the obtained value of transmission loss is approximately maintained up to ~(-3.0-0.3) dB for $D_2$=7.3 mm and 7.6 mm for frequency from 9.5 GHz to 14 GHz. For lower in-band frequency range from 7 to 9.5 GHz the value for transmission loss is approximately -2.5 dB which may be due to imbalance at lower band. For other values of $D_2$, transmission loss increases up to 4 dB, which shows performance degradation. Figure 4(b) demonstrates the graph for power coupled to coupling port (port 4) for the designed coupler with respect to frequency range of 7-14 GHz.

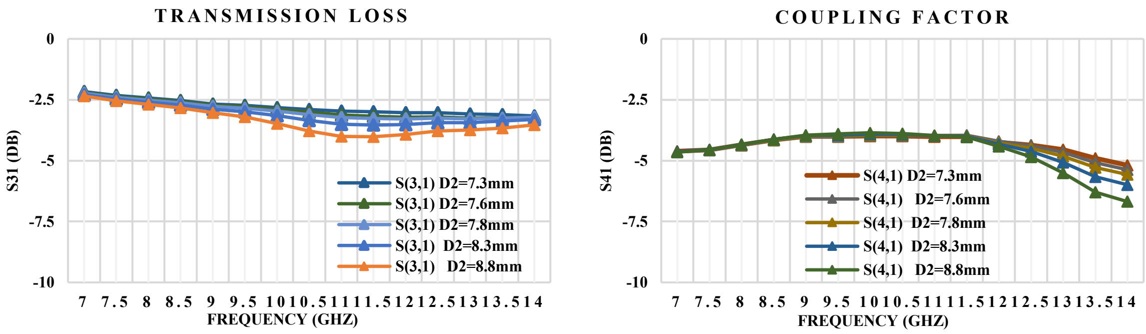


(a) (b)

Figure 4. Comparative plots of simulated; (a) transmission loss (S31) and (b) coupling factor of the designed directional coupler for different values of slot diameter $D_2$

At the optimized dimensions of ($D_1$=3.8 mm) and ($D_2$=7.3 mm), the proposed coupler achieves a coupling factor of -3.88 dB at the center frequency of 10.5 GHz. Across the 7–14 GHz frequency range, the coupling remains within approximately (-4±0.8 dB), indicating stable coupling performance over the desired bandwidth. The corresponding parametric performance is presented in Figures 3 and 4. The following section provides a detailed analysis of the remaining performance parameters for the optimized coupler configuration.

### 3.1.2. Simulation results for $D_2$=7.3 mm

The simulation results for the optimal case of $D_2$=7.3 mm are shown in Figures 5 to 7. Figure 5 shows the simulation results for return loss and isolation under optimized conditions. On observing the return loss in Figure 5(a), it is seen that for frequency range 7 to 10 GHz the value is maintained below -20 dB. For frequency range from 10 to 14 GHz the return loss is maintained better than 15 dB, ensuring minimal signal reflection at the input over the wideband range. The Ports 1 and 2 are the isolation ports.

In Figure 5(b), the simulated results show that around the center frequency, the isolation is better than 22 dB and over the whole bandwidth the isolation is better than 16 dB. As the frequency increases, the electrical length of the coupler's features changes, and parasitic effects become more pronounced. The most probable cause is a combination of phase velocity mismatch and the increasing impact of geometric discontinuities at higher frequencies. Considering the wideband operation, the isolation is decent.

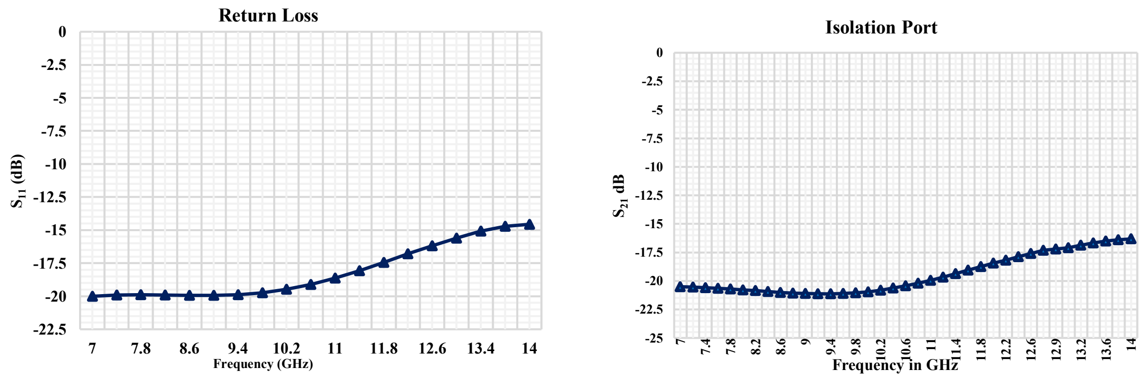


(a) (b)

Figure 5. Simulation result for; (a) return loss ($S_{11}$) and (b) isolation ($S_{21}$) versus frequency for the proposed directional coupler for slot diameter $D_2$=7.3 mm

The simulated input voltage standing wave ratio (VSWR) for the proposed directional coupler is shown in Figure 6. At its optimized elliptical slot diameter of $D_2$=7.3 mm, demonstrates good broadband impedance matching across the entire operational band. The VSWR values consistently remain between 1.22

and 1.46. This strong performance directly corresponds to a return loss better than 14.5 dB across the spectrum, validating the effectiveness of the elliptical geometry and confirming the design's suitability for high-performance UWB systems where efficient power transfer is paramount. Which is a critical indicator of high signal integrity and ensures maximum power transfer by minimizing reflections at the input port.

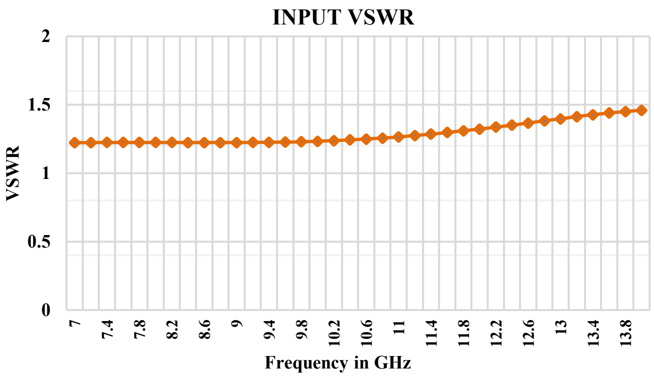


Figure 6. Simulated input VSWR of the proposed directional coupler for $D_2$=7.3 mm across the operating frequency band

In Figure 7(a), the transmission loss is approximately maintained at 3.3±0.4 dB, the transmission loss is ~2.95 dB for frequency 7 to 8.2 GHz, after that for frequency range 11.5 to 12.5 GHz the loss dips to 3.3 dB. From 13 to 14 GHz again the transmission loss becomes ~2.8 dB. The multilayer substrate design contributes to the transmission loss. Figure 7(b) confirms that the coupling factor remains within −3.5±0.4 dB across the entire frequency range. It can be observed that the coupling factor is decreased to -3.78 dB between 11.5 to 14 GHz frequency band; this can be attributed to degradation in isolation for the upper band.

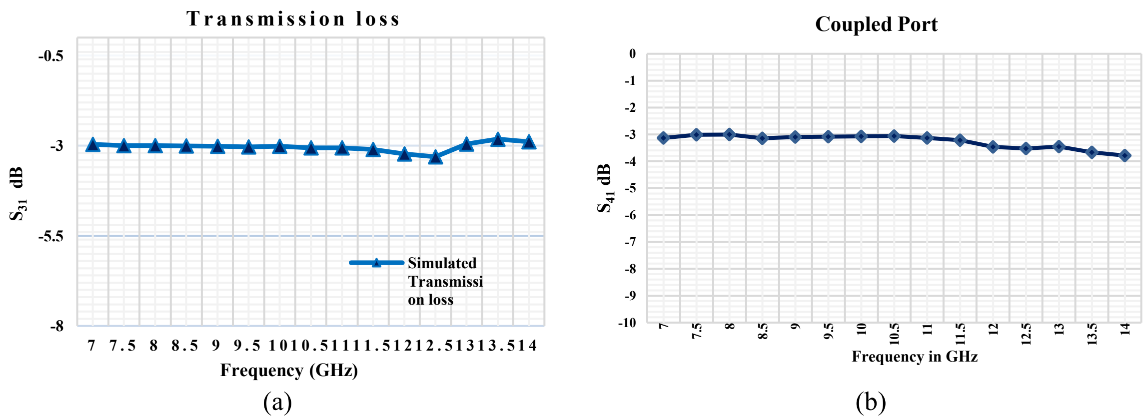


Figure 7. Simulation result for; (a) transmission loss ($S_{31}$) and (b) coupling factor ($S_{41}$) versus frequency for the proposed directional coupler for slot diameter $D_2$=7.3 mm

From the above analysis, it has been inferred that the optimal simulated performance of the proposed coupler was achieved with an elliptical slot dimension of $D_2$=7.3 mm. Table 1 summarizes the simulated S-parameters and performance metrics of the proposed elliptical multilayer directional coupler at the optimal slot dimension ($D_2$=7.3 mm). With good return loss, high isolation, minimal insertion loss, and reliable coupling, these results show that the proposed coupler configuration works well over a wide frequency range. Therefore, the design meets the main needs for effective X-band directed coupling in small and wideband microwave systems.

Table 1. Summary of simulation results at $D_2$=7.3 mm

| Parameter | Value/range | Remarks |
|---|---|---|
| Return loss ($S_{11}$) | ≥15 dB, peak at 20 dB | Excellent impedance matching |
| Transmission loss ($S_{31}$) | 3.3±0.4 dB | Min. at 7.3 mm; increases after |
| Isolation ($S_{21}$) | ≥-16.5 dB, peak at -22 dB | Adequate P1–P2 isolation |
| Coupling factor ($S_{41}$) | −3.5±0.6 dB | Stable coupling across band |
| VSWR | 1.22 to 1.46 | Indicates good impedance matching |
| Optimal slot diameter (major axis) $D_2$ | 7.3 mm | Best overall trade-off |

### 3.2. Performance verification of the fabricated prototype

The designed microstrip directional coupler was fabricated using conventional photolithography and PCB etching procedures, the prototype was brought to life on a TLY-5 substrate, specifically selected for its low-loss properties. To validate the performance of the fabricated directional coupler, a full four-port characterization was conducted by measuring its scattering parameters. The S-parameters were measured over a frequency range of 7-14 GHz using a Keysight N5222A VNA. Experimental testing with a calibrated VNA confirmed the results of the simulations for the proposed elliptical multilayer directional coupler. The manufactured prototype and the associated test apparatus for S-parameter measurements are shown in Figure 8. The Figure 8(a) shows the photograph of the fabricated prototype of the 3 dB elliptical multilayer directional coupler. Top view of the device, showing the microstrip lines on an TLY-5 substrate. Key features, including the input/output ports and the parallel coupling section, are indicated. A 2 Rupee coin is placed alongside for scale comparison. Figure 8(b) demonstrates the test setup for S-parameter measurement of the microstrip directional coupler. The device under test (DUT) is connected between Port 1 and Port 2 of a Keysight N5222A VNA. The coupled (Port 4) and isolated (Port 3) ports of the DUT are terminated with 50 Ω loads to ensure accurate measurement. The arrows indicate the direction of signal flow for the S21 measurement.

(a) (b)

Figure 8. Fabricated coupler and measurement setup; (a) proposed elliptical multilayer directional coupler and (b) S-parameter measurement using a Keysight N5222A VNA with 50 Ω terminations

As a 3 dB directional coupler, the device is designed for an equal power split. The coupling factor ($S_{41}$), transmission loss ($S_{31}$), and return loss ($S_{11}$) were the primary S-parameters that were experimentally evaluated and compared with their simulated equivalents to confirm the accuracy of the design. The measured S-parameters were compared with the simulated data. Figures 9 and 10 present these comparative plots. The difference in transmission loss ($S_{31}$) between the simulation and measurement is illustrated in Figure 9(a). Across all frequencies, the measured transmission loss maintains around -2.7-0.5 dB, which is in good match with the performance that was expected. Factors such as parasitic effects caused by SMA connections and soldering pads, substrate dielectric losses, and conductor surface roughness contribute for the difference. This is common in real-world RF testing settings and usually causes the measured losses to be slightly larger than the idealized calculations.

The simulated and measured coupling factor ($S_{41}$) spanning over the 7-14 GHz frequency spectrum is compared in Figure 9(b); it can be observed that the coupling level remains about $-3.5 \pm 0.6$ dB, and the measured results show a strong agreement with the simulated data. Practical considerations including fabrication tolerances, via misalignments, and connector mismatches account for the minor discrepancies seen at lower band edge frequencies and higher band edge frequencies.

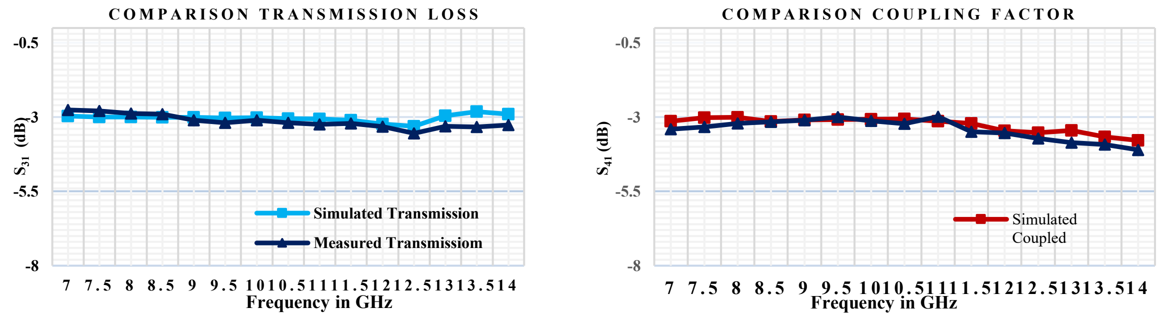


(a) (b)

Figure 9. Comparison of simulated and measured; (a) transmission loss ($S_{31}$) and (b) coupling factor versus frequency for the fabricated directional coupler, showing good agreement

Figure 10 shows the comparative performance of simulated and measured return loss and isolation. In Figure 10(a), the return loss performance is illustrated. At the 10.5 GHz center frequency, the measured $S_{11}$ values approach 20 dB, indicating excellent impedance matching, and they maintain over 12 dB for the majority of the operational spectrum. Near the band boundaries, however, return loss shows a small decline. The main reasons for these differences are the air gaps between the layers of the substrate, small misalignments between the layers, and manufacturing flaws that are hard for simulation models to adequately illustrate. Figure 10(b) shows the comparative graph of the simulated and measured isolation. The measured isolation is in close agreement with the simulated value, but there is uniform degradation in the isolation value as compared to simulation.

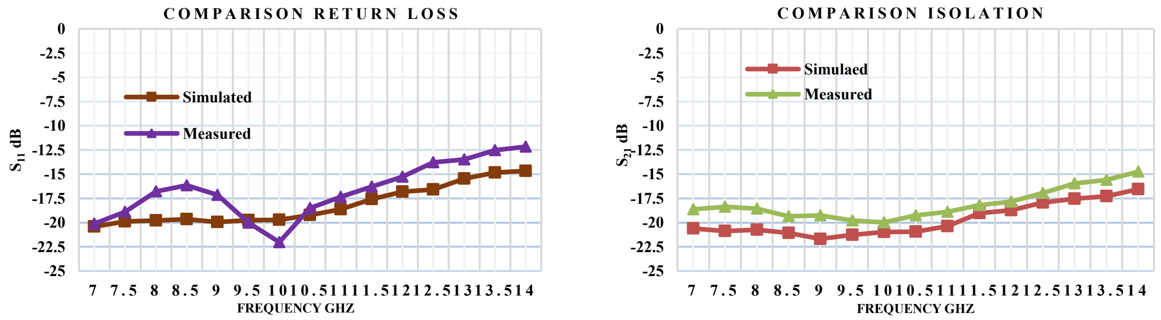


(a) (b)

Figure 10. Comparison of the simulated and measured; (a) return loss ($S_{11}$) and (b) isolation loss ($S_{21}$) responses of the fabricated coupler, showing a measured return loss of −22.5 dB and isolation of −19.26 dB at 10 GHz

### 3.2.1. Validation and analysis

The measured S-parameters show that the proposed 3 dB coupler achieves nearly equal power division at 10.5 GHz, with $S_{21}$=−3.18 dB and $S_{31}$=−3.22 dB, corresponding to only 0.03 dB imbalance. Over the 7–14 GHz band, the insertion loss varies from -2.7 dB to -3.3 dB. The multilayer design also offers good isolation: simulations predicted better than -16 dB across the band and -22 dB at 10.5 GHz, while the fabricated TLY-5 prototype measured about -19 dB in the mid-band, degrading to -16 dB near 14 GHz.

This discrepancy highlights the effect of fabrication and material tolerances at high frequencies. Small variations in dielectric constant, anisotropy, etching, and structural asymmetry disturb field symmetry and prevent ideal even- and odd-mode phase velocity equalization. As a result, the measured isolation degrades, reducing the directivity from the simulated 17 dB to 15 dB at the center frequency. Similarly, although the measured return loss reaches -18.5 dB at the center frequency, it degrades to about -12 dB over 11–14 GHz, indicating higher frequency sensitivity of the fabricated prototype compared to the ideal model. A comparison between the simulated and measured results is provided in Table 2.

Table 2. Comparison of simulation and measurement parameters of proposed coupler

| Parameter | Frequency (GHz) | Simulation | Measured | Difference (Δ) |
|---|---|---|---|---|
| Transmission loss (dB) | | | | |
| - Center frequency | 10.5 | -3.055 | -3.1189 | -0.13363 |
| - Band edge low | 7 | -2.96606 | -2.7587 | 0.207 |
| - Band edge high | 14 | -2.8946 | -3.26667 | -0.372 |
| Return loss (dB) | 10.5 | -19.2089 | -18.5089 | -0.7 |
| Coupling (dB) | 10.5 | -3.058 | -3.2189 | -0.2 |
| Isolation (dB) at center freq | 10.5 | -20.92 | -19.26 | -1.66 |
| Directivity (dB) | 10.5 | 17 | 16 | 1 |

The experimental results provide strong validation for the simulated elliptical multilayer UWB directional coupler, confirming its robust performance across the 7-14 GHz spectrum. The device successfully achieves an excellent balance between its compact physical footprint of 2.475 λg×1.485 λg and high-fidelity signal integrity. Key measured metrics include a return loss exceeding 12 dB across the entire band, a peak isolation of 22 dB at the 10.5 GHz center frequency, and a highly stable coupling factor of −3.5 ±0.6 dB, which confirms uniform power division—a critical attribute for advanced systems. The strong correlation between measurement and simulation validates the design's precision, with minor, predictable discrepancies at the band edges credibly attributed to practical fabrication challenges such as inter-layer air gaps and connector parasitics. A comparative analysis against recently published works confirms that the proposed coupler offers significant advantages in performance and size. This analysis considers key performance metrics such as return loss ($S_{11}$), insertion loss ($S_{21}$), coupling factor ($S_{41}$), isolation, FBW, and overall footprint. The suggested elliptical multilayer directional coupler demonstrates significant benefits in these measures. Table 3 summarizes the findings of the comparisons made between the proposed coupler and other designs by other researchers.

The proposed design demonstrates good signal integrity, with a return loss exceeding 12 dB over the entire frequency spectrum, with isolation levels attaining 22 dB at the central frequency of 10.5 GHz. The measured transmission loss of approximately ~3 dB as expected for a 3 dB coupler. The result is comparable to most systems documented in the literature, signifying enhanced power transfer efficiency. Moreover, the coupling factor of −3.5± 0.6 dB is robust and uniform throughout the 7–14 GHz spectrum, confirming the elliptical geometry's contribution to stable and broadband coupling.

Table 3. Comparative performance of proposed design with existing directional coupler

| Author(s) | Return loss (dB) | Insertion loss (dB) | Coupling (dB) | Isolation (dB) | FBW (%) | Frequency range (GHz) | Technology |
|---|---|---|---|---|---|---|---|
| Abdulbari *et al.* [4] | 28 | 3 | 3 | 29 | 20 | 0.905–1.105 | T-shape with open stub microstrip line |
| Rabbanifard *et al.* [5] | 12 | 3 ± 1 | 3 ± 0.8 | 12 | 40 | 20–30 | Cross-shaped groove gap waveguide |
| Nguyen *et al.* [6] | >10 | −3.3 | −6.0 | >20 | 30 | 8.6–11.6 | SIW directional coupler with isolation-enhancing aperture |
| Tian *et al.* [7] | 43.7 | 3.07 | 3.04 | 15 | – | 0.3–0.7 | CMCPW |
| Maheswari and Jayanthy [10] | 16.6 | 3.54 | 3.57 | 20.8 | – | 1.4–3 | Pi network with shunt Capacitance |
| Roshani *et al.* [13] | 20 | 3.6 ± 0.5 | 3.6 ± 0.5 | 20 | 49 | 4.5–7.4 | T-shaped resonators, open stubs, cross-shaped resonators and radial stubs |
| Herraiz *et al.* [21] | 30.69 | 2.97 | 3.65 | 29.3 | 30.2 | 2–5 | ESICL technology |
| Patel *et al.* [24] | (>16) | 8.3 | 0.45–1.62 | (>20) | 133.3 | 0.75–3.75 | Three-section microstrip coupler |
| Proposed work | 21.5 | 3.3± 0.4 | 3.5 ± 0.6 | 22 | 66.6 | 7–14 | Multilayer substrate microstrip |

The fabricated 7–14 GHz directional coupler, with a measured FBW of 66.7%, is suitable for various UWB microwave applications. In its optimal 9–11.5 GHz sub-band, its high isolation and good amplitude balance make it well suited for I/Q modulators, balanced amplifiers, and phased-array feed networks. Over the full band, it can also be used in UWB radar and spectrum monitoring systems, where edge-band degradation may be compensated through system-level calibration. In addition, it provides a suitable foundation for reflective variable attenuator design, since its isolation and directivity directly influence the attenuator performance.

## 4. CONCLUSION

A compact wideband multilayer elliptical directional coupler for X-band applications has been designed, simulated, fabricated, and experimentally validated. The proposed coupler operates over 7–14 GHz with a measured FBW of 66.6%, while providing a coupling level of about −3.5±0.6 dB, insertion loss of nearly 2.9 dB, return loss greater than 20 dB at the center frequency, and isolation around 22 dB. These results confirm that the proposed structure is suitable for broadband signal monitoring and power sampling applications. In addition, comparison with recent reported designs demonstrates its advantages in terms of compactness, bandwidth, and overall performance. The achieved results also indicate that the proposed coupler can serve as a promising building block for future reflective variable attenuator design, where its coupling and isolation characteristics may be effectively utilized to realize controllable wideband attenuation.

## FUNDING INFORMATION

Authors state no funding involved.

## AUTHOR CONTRIBUTIONS STATEMENT

This journal uses the Contributor Roles Taxonomy (CRediT) to recognize individual author contributions, reduce authorship disputes, and facilitate collaboration.

| Name of Author | C | M | So | Va | Fo | I | R | D | O | E | Vi | Su | P | Fu |
|---|---|---|---|---|---|---|---|---|---|---|---|---|---|---|
| Shilpa Ankit Rana | ✓ | ✓ | ✓ | ✓ | ✓ | ✓ | ✓ | ✓ | ✓ | ✓ | | | | |
| Ashish Kalubhai Sarvaiya | | | | | | ✓ | | | | ✓ | | ✓ | | |

C : **C**onceptualization
M : **M**ethodology
So : **So**ftware
Va : **Va**lidation
Fo : **Fo**rmal analysis
I : **I**nvestigation
R : **R**esources
D : **D**ata Curation
O : Writing - **O**riginal Draft
E : Writing - Review & **E**diting
Vi : **Vi**sualization
Su : **Su**pervision
P : **P**roject administration
Fu : **Fu**nding acquisition

## CONFLICT OF INTEREST STATEMENT

The authors have no conflicts of interest to declare.

## DATA AVAILABILITY

Data availability is not applicable to this paper as no new data were created or analyzed in this study.

## REFERENCES

[1] C. Mier, A. R. Mor, and P. Vaessen, "A directional coupler for partial discharge measurements in gas-insulated substations," *Measurement*, vol. 225, Feb. 2024, doi: 10.1016/j.measurement.2023.113996.
[2] A. M. Abbosh and M. E. Bialkowski, "Design of Compact Directional Couplers for UWB Applications," *IEEE Trans. Microw. Theory Tech.*, vol. 55, no. 2, pp. 189–194, Feb. 2007, doi: 10.1109/TMTT.2006.889150.
[3] K. Abouhssous, A. Zugari, and A. Zakriti, "A Comprehensive Review of Planar Directional Coupler Performance Improvement Techniques," *Telecommun. Radio Eng. (English Transl. Elektrosvyaz Radiotekhnika)*, vol. 81, no. 9, pp. 23–58, 2022, doi: 10.1615/TelecomRadEng.2022043704.
[4] A. A. Abdulbari, S. K. A. Rahim, M. Z. A. A. Aziz, K. G. Tan, N. K. Noordin, and M. Z. M. Nor, "New design of wideband microstrip branch line coupler using T-shape and open stub for 5G application," *Int. J. Electr. Comput. Eng.*, vol. 11, no. 2, pp. 1346–1355, Apr. 2021, doi: 10.11591/ijece.v11i2.pp1346-1355.
[5] M. Rabbanifard, D. Zarifi, A. Farahbakhsh, and M. Mrozowski, "Design of Compact and Wideband Groove Gap Waveguide-Based Directional Couplers," *IEEE Access*, vol. 12, pp. 86346–86354, 2024, doi: 10.1109/ACCESS.2024.3416290.
[6] T.-L. Nguyen *et al.*, "SIW Directional Coupler with Improved Isolation for X-Band Applications," *Electronics*, vol. 14, no. 4, pp. 1-12, Feb. 2025, doi: 10.3390/electronics14040774.
[7] H. Tian, K. L. Chung, R. Liu, M. Dai, and W. Tang, "Miniaturised quadrature hybrid coupler using composite planar transmission lines," *Electron. Lett.*, vol. 55, no. 19, pp. 1049–1051, Sep. 2019, doi: 10.1049/el.2019.1704.
[8] A. Lalbakhsh *et al.*, "Design of a Compact Planar Transmission Line for Miniaturized Rat-Race Coupler With Harmonics Suppression," *IEEE Access*, vol. 9, pp. 129207–129217, 2021, doi: 10.1109/ACCESS.2021.3112237.
[9] M. Salehi and L. Noori, "Novel 2.4 Ghz branch-line coupler using microstrip cells," *Microw. Opt. Technol. Lett.*, vol. 56, no. 9, pp. 2110–2113, Sep. 2014, doi: 10.1002/mop.28552.
[10] S. Maheswari and T. Jayanthy, "Design of Compact Branch-Line Coupler for Wi-Max Applications," *Int. J. Microw. Opt. Technol.*, vol. 17, no. 1, pp. 68–73, 2022.

[11] W. A. Arriola, J. Y. Lee, and I. S. Kim, "Wideband 3 dB Branch Line Coupler Based on $\lambda/4$ Open Circuited Coupled Lines," *IEEE Microw. Wirel. Components Lett.*, vol. 21, no. 9, pp. 486–488, Sep. 2011, doi: 10.1109/LMWC.2011.2138687.

[12] N. A. M. Shukor and N. Seman, "Enhanced Design of Two-Section Microstrip-Slot Branch Line Coupler with the Overlapped $\lambda/4$ Open Circuited Lines at Ports," *Wirel. Pers. Commun.*, vol. 88, no. 3, pp. 467–478, Jun. 2016, doi: 10.1007/s11277-015-3138-z.

[13] S. Roshani, S. I. Yahya, S. Roshani, A. H. Farahmand, and S. Hemmati, "Design of a Modified Compact Coupler with Unwanted Harmonics Suppression for L-Band Applications," *Electronics*, vol. 11, no. 11, pp. 1-15, May 2022, doi: 10.3390/electronics11111747.

[14] A. Rezaei, S. I. Yahya, and L. Nouri, "A Comprehensive Review on Microstrip Couplers," *ARO-THE Sci. J. KOYA Univ.*, vol. 11, no. 1, pp. 22–31, Jan. 2023, doi: 10.14500/aro.11108.

[15] M. Yayan and A. C. Yapici, "Design of wideband multi-layer quadrature hybrid couplers with butterfly-shaped resonators," *Int. J. Microw. Wireless Technol.*, vol. 14, no. 7, pp. 815–823, 2022, doi: 10.1017/S1759078721000969.

[16] M. A. Abbas, A. M. Allam, A. Gaafar, H. M. S. El-Hennawy, and M. F. A. Sree, "A 3-dB compact UWB hybrid coupler for 5G millimeter-wave applications," *Prog. Electromagn. Res. C*, vol. 135, pp. 23–34, 2023.

[17] U. Shah, M. Sterner, and J. Oberhammer, "High-directivity MEMS-tunable directional couplers for 10–18-GHz broadband applications," *IEEE Trans. Microw. Theory Techn.*, vol. 61, no. 9, pp. 3236–3246, Sep. 2013, doi: 10.1109/TMTT.2013.2273763.

[18] H. Abedi, M. M. Taskhiri, and E. Hadian, "Design and analysis of multi-layer SIW coupler to use in phased array antenna feed network," *J. Eng.*, vol. 2023, 2023, doi: 10.1049/tje2.12235.

[19] M. You, G. Liu, and Z. Cheng, "Analysis and design of weak coupling coupler based on the half mode substrate integrated waveguide," *Int. J. Microw. Wireless Technol.*, vol. 15, no. 5, pp. 734–741, Jun. 2023, doi: 10.1017/S1759078723000156.

[20] B. Tegowski and A. Koelpin, "Multilayer substrate integrated waveguide six-port junctions with embedded resistive films," *Int. J. Microw. Wireless Technol.*, vol. 17, no. 2, pp. 285–293, Mar. 2025, doi: 10.1017/S1759078724000680.

[21] D. Herraiz *et al.*, "High-Directivity and Low-Loss Directional Couplers Based on Empty Substrate Integrated Coaxial Line Technology," *IEEE Access*, vol. 12, pp. 35630–35642, 2024, doi: 10.1109/ACCESS.2024.3371701.

[22] S.-L. Liu and L. Liu, "A compact directional coupler with high directivity using ferrite components," *Electron. Lett.*, vol. 59, no. 12, 2023, doi: 10.1049/ell2.12849.

[23] F. Zhu, X. Zhao, J. Sheng, and G. Q. Luo, "Broadband and compact folded substrate integrated waveguide phase shifter and its application to 180° directional coupler," *Int. J. Microw. Wireless Technol.*, vol. 15, no. 4, pp. 554–559, May 2023, doi: 10.1017/S1759078722000915.

[24] S. K. Patel, R. K. Barik, N. K. Dewangan, and S. Koziel, "Design and experimental validation of multi-section directional coupler with arbitrary coupling and high directivity for sub-6 GHz UWB applications," *PLoS One*, vol. 21, no. 5, May 2026, doi: 10.1371/journal.pone.0347748.

[25] L. Riaz *et al.*, "Electronically tunable half-mode substrate-integrated waveguide coupler," *IEEE Access*, vol. 14, pp. 9183–9192, 2026, doi: 10.1109/ACCESS.2026.3654176.


## BIOGRAPHIES OF AUTHORS

**Prof. Shilpa Ankit Rana** is an Assistant Professor at Government Engineering College with over 15 years of teaching experience. She holds a B.E. in Electronics and Communication from Gujarat University and an M.Tech. from DDU, Nadiad, and is currently pursuing a Ph.D. at Gujarat Technological University. Her research interests include RF and microwave circuits, antenna design, and wireless communication. She can be contacted at email: shilparana7187@gmail.com.

**Dr. Ashish Kalubhai Sarvaiya** is an Assistant Professor at Government Engineering College, Bhavnagar. He holds a B.E. in Electronics and Communication, an M.E. in Microwave Engineering, and a Ph.D. from Dhirubhai Ambani Institute of Information and Communication Technology. With over 20 years of academic experience, his research interests include computational electromagnetics, EMC/EMI, RF and microwave circuits, and antennas. He is also a recognized Ph.D. supervisor under Gujarat Technological University. He can be contacted at email: aks_441@yahoo.co.in.